HHS Public Access

Author manuscript

Acad Radiol. Author manuscript; available in PMC 2015 June 24.

Published in final edited form as:

Acad Radiol. 2014 June ; 21(6): 817–823. doi:10.1016/j.acra.2014.02.001.

Geometric Distortion in Diffusion-weighted MR Imaging of the Prostate—Contributing Factors and Strategies for Improvement

Francisco Donato Jr., MD, **Daniel N. Costa, MD**, **Qing Yuan, PhD**, **Neil M. Rofsky, MD**, **Robert E. Lenkinski, PhD**, and **Ivan Pedrosa, MD**

Department of Radiology, University of Texas Southwestern Medical Center, 5323 Harry Hines Blvd, Dallas, TX 75390-9061

Daniel N. Costa: Daniel.Costa@UTSouthwestern.edu

Abstract

Rationale and Objectives—Image distortion on diffusion-weighted imaging (DWI) of the prostate in 3T endorectal magnetic resonance imaging (MRI) examinations is common. The aim of this study was to determine the degree of distortion on DWI using a state-of-the-art clinical protocol and to explore the main contributors to geometric distortion.

Materials and Methods—Forty consecutive patients underwent 3T MRI of the prostate with an endorectal coil filled with air (n = 20) or barium sulfate (n = 20). Distortion was measured as the maximum displacement of the outer boundary of the prostate on DWI relative to T2-weighted imaging. The effects of phase-encoding direction, receiver bandwidth, and parallel imaging were then assessed in a prostate phantom on two MRI scanners from different manufacturers.

Results—There was no statistical difference in the mean displacement of the prostate on DWI between the air cohort (1.8 ± 1.2 mm, range 0–4.2 mm) and barium cohort (1.8 ± 2.2 mm, range 0–9 mm). Displacement of the prostate was observed in the phase-encoding direction. Phantom experiments demonstrated a horizontal displacement of 6.0 mm in the phase-encoding direction, which decreased with the use of parallel imaging and higher bandwidth. Geometric distortion was similar for all b values and across manufacturers.

Conclusions—Geometric distortion on DWI of the prostate is common in the phase-encoding direction and does not improve with inflating the coil with barium sulfate. Strategies to reduce this artifact include the use of higher bandwidth and accelerated imaging. Correction of this phenomenon should improve localization of prostate cancer, particularly important for targeted prostate biopsies or focal therapies.

Keywords

MRI; diffusion-weighted imaging; prostate cancer; artifacts; image registration

Diffusion-weighted imaging (DWI) has become a key component of multiparametric magnetic resonance imaging (mpMRI) of the prostate (1). Although DWI improves prostate cancer detection (2–4) and apparent diffusion coefficient (ADC) values derived from these

Correspondence to: Daniel N. Costa, Daniel.Costa@UTSouthwestern.edu.

acquisitions seem to correlate with tumor grade (5,6) potentially predicting disease aggressiveness, this technique is prone to image distortion (7).

DWI relies on multiple acquisitions, probing the rate with which water diffuses in various directions and over different scales. Although single-shot spin-echo echo-planar imaging (SE-EPI) is very sensitive to magnetic field inhomogeneities, such as those caused by air in the rectum or within the endorectal coil (ERC) near the prostate (8,9), it is the most commonly used sequence in DWI. With SE-EPI, phase error accumulation results in voxel shifts that distort the image along the phase-encoding direction (7). New gradient coils capable of extremely fast linear gradient switches have enabled DWI acquisition with higher spatial resolution. However, increasing the resolution results in longer echo trains and further increases the accumulation of errors during the spatial encoding (8).

The more recent development of techniques for MRI-targeted biopsy and focal therapy has generated a clinical need for improving tumor localization with imaging (10). In clinical practice, we have observed the presence of geometric distortions causing displacement of structures on DWI images relative to fast spin-echo T2-weighted images (T2-FSE). Although several studies address geometric distortion on DWI of other organs (7,8,11,12), this topic has not been explored in the prostate to our knowledge. Understanding the factors that influence image distortion on DWI of the prostate is the first step in developing solutions. Moreover, the use of barium sulfate to inflate the balloon of the ERC decreases susceptibility gradients in prostate examinations and improves spectroscopic acquisitions, similarly to the results obtained with perfluorocarbon (9). However, to our knowledge, the effect of inflating the ERC with barium sulfate on the distortion artifacts in DWI has not been investigated. The purpose of this study was to identify the causes and degree of geometric distortion observed in DWI of the prostate in human studies and phantom experiments and to assess different acquisition strategies to decrease the distortion, including inflation of the ERC with air versus barium sulfate.

MATERIALS AND METHODS

Patient Selection and MRI Protocol

During the first stage of this investigation, we retrospectively reviewed 40 consecutive mpMRI prostate studies performed between November 2011 and September 2012, on a 3T MRI scanner (Achieva TX; Philips Medical Systems, Best, The Netherlands) with a six-element cardiac coil (Philips Medical Systems) and an ERC (Medrad, Warrendale, PA). The balloon of the ERC was initially filled with 50 cc of air at our institution. Later, our clinical protocol was changed, and the ERC was inflated with 50 cc of barium sulfate (Polibar Plus, E-Z-EM, Lake Success, NY) based on prior reports indicating a potential advantage of this approach in reducing susceptibility artifacts (9). We included in this study the last 20 consecutive patients in whom the coil was inflated with air (*air cohort*) and the next 20 consecutive patients in whom we changed to barium filling (*barium cohort*). The MRI protocol parameters were not modified during the study period. Axial DWI images of the prostate were acquired using an SE-EPI sequence with echo time (TE)/repetition time (TR) of 75–78/6776–6955 milliseconds, slice thickness 3 mm with gap 0.3 mm, field of view (FOV) 180 × 180 mm^2, matrix 144 × 140, bandwidth of 1267– 1392 Hz/pixel, phase-

encoding direction right-to-left, echo train length of 73, SENSE factor of 2, and *b* values 0, 50, 1000, and 1500 s/mm^2, total number of averages = 3 for *b* = 0 and *b* = 50, and 6 for *b* = 1000 and *b* = 1500, scan time 5 minutes 41 seconds. Axial T2-FSE images of the prostate were acquired with the same orientation and phase-encoding direction, TE/TR of 120/7878–10233 milliseconds, slice thickness 2.5–3.0 mm and no gap, FOV 180 × 180 mm^2, acquisition matrix 392 × 312, bandwidth of 218–250 Hz/pixel, echo train length of 25–26, SENSE factor of 2. Coronal and sagittal T2-FSE and dynamic contrast-enhanced spoiled gradient echo images were also acquired as part of the clinical protocol but not used for the purpose of this retrospective study.

Phantom Experiments

The second phase of this study used a multimodality prostate phantom model (Yezitronix Group Inc., Quebec, Canada; Fig 1). Phantom MRI acquisitions were obtained on the same MRI scanner and the same combination of cardiac coil and ERC as in patients. Experiments were carried out with the ERC filled with 50 cc of barium sulfate or air. The axial DWI images were acquired using an SE-EPI sequence with TE/TR of 76–99/10000 milliseconds, slice thickness 3 mm with gap 0.3 mm, FOV 160–180 × 160–180 mm^2, matrix 128–144 × 124–141, bandwidth of 751–1526 Hz/pixel, echo train length of 65–141, SENSE factor of 1–2, and *b* values 0, 50, 500, 1000, and 1500 s/mm^2. Axial T2-FSE images with TE/TR of 120/8000 milliseconds, acquisition matrix 348–392 × 260–312, bandwidth of 231–236 Hz/pixel, echo train length of 26, SENSE factor of 2, with the same slice thickness, gap, and FOV as for the DWI images, were acquired at the same locations and used as the standard of reference. For both sequences, the phase-encoding direction was right-to-left unless specifically modified as discussed in the following. T2-FSE was chosen as reference for anatomy because in this sequence one k-space line is acquired per phase-encoding step; thus, the effects of the field inhomogeneities in these images are negligible (7).

Four tests were performed separately on the phantom studies changing only the feature indicated and holding all other parameters as indicated previously: (1) the phase-encoding direction was changed from right-to-left to anterior-to-posterior; (2) the fat-shift direction was inverted, therefore inverting the polarity of the diffusion gradients; (3) bandwidth was increased from 751 to 1252 Hz/pixel (by changing the water fat-shift from maximum to minimum); and (4) acceleration (SENSE) factor was increased from 1 to 2. Other acquisition parameters were not changed. The same experiments were repeated on a different 3T MRI scanner (Signa HDxt; GE Healthcare, Milwaukee, WI) using similar MRI protocol and imaging parameters.

Image Analysis

Images from MRI examinations were retrospectively reviewed using open-source software (Osirix; Osirix Foundation, Geneva, Switzerland). The outer contour of the prostate gland was manually drawn and saved by one of the investigators (FDJ, a radiologist with 6 years of training) on the T2-FSE images and each of the five DWI images (*b* = 0–1500) using free-hand regions of interest (ROIs). T2-FSE and DWI images were selected at the same level through the middle of the gland, using spatial coordinates and coronal T2-FSE images as reference. The displacement between the T2-FSE images and the DWI images was used

as a surrogate of geometric distortion. This displacement was determined by overlaying the saved ROI representing the prostate contour from the T2-FSE images on the DWI images and measuring the maximum distance between the boundaries in a left–right (horizontal) direction. The anterior–posterior displacement was noted to be consistently <1 mm and therefore was not included in the analysis (Fig 2). A similar image analysis was performed for the phantom experiments.

Statistical Analysis

In the patient cohort, Friedman test was used to assess the difference in mean displacement between the T2-FSE and DWI images for the barium and air cohorts adjusted by *b* values; one sample nonparametric sign rank test and two sample Wilcoxon rank sum test (with continuity correction) were used to test the difference between the means. All analyses were performed using SAS software version 9.2 (SAS Institute, Cary, NC). A *P* value <.05 was considered statistically significant.

Our Institutional Review Board approved this study.

RESULTS

In patients, a mean displacement of 1.8 mm (standard deviation [SD] 1.2 mm; range 0–4.2 mm) was observed in the phase-encoding direction when the ERC was inflated with air compared to 1.8 mm (SD 2.2 mm; range 0–9.0 mm) when the ERC was inflated with barium sulfate. There was no significant difference in the displacement for low or high *b* values (*P* value = .53) or between the air and barium cohorts (*P* value = .22; Table 1). The displacement in the frequency-encoding direction was negligible.

In the phantom experiments with barium-filled ERC, geometric distortion was also observed in the phase-encoding direction with an initial displacement of 6.0 mm on the DWI images compared to the T2-FSE images. The displacement decreased from 6.0 to 4.0 mm by increasing the SENSE factor from 1 to 2 (Fig 3). The displacement decreased from 4.0 to 2.9 mm by increasing the bandwidth from 751 to 1252 Hz/ pixel (Fig 4). The geometric distortion was similar for all *b* values from 0 to 1500 (Fig 5). The distortion switched from the right–left to the anterior–posterior axis following a similar change in the phase-encoding axis. In both axes, the distortion orientation was inverted by inverting the fat-shift direction (Fig 6). Table 2 presents the MRI parameters and their effects in the geometric distortion on a phantom model. No perceptible difference was noted between inflating the ERC with air or barium sulfate. These results were reproduced on both 3T MRI scanners.

DISCUSSION

Our results confirm an average displacement of the prostate on DWI acquisitions compared to T2-weighted FSE acquisitions of almost 2 mm, using a state-of-the-art clinical 3T MRI protocol with ERC. Geometric distortions on SE-EPI DWI of the prostate occur in the phase-encoding direction. The distortion in the readout direction was however negligible. That was confirmed by shifting the phase- and frequency-encoding axes. Using higher bandwidth and accelerated imaging reduced the degree of distortion along the phase-

encoding direction. By repeating the experiment on different scanners, we demonstrated that the distortion occurs irrespective of the manufacturer.

Our results support the finding that geometric distortion in EPI is mainly caused by the accumulation of phase error over the phase-encoding direction during the slice acquisition, leading to voxel shifts almost exclusively in this direction (11). Investigation by Jezzard et al. (11) found the fact that the geometric distortions in EPI are mainly caused by the presence of an inhomogeneous main magnetic field (*B*0). Accordingly, the geometric distortion (Δy) at a position (x, y, z) is calculated by:

$$\Delta y_{(x,y,z)} = \gamma \Delta B_{(x,y,z)} \mathrm{FOV}_y / \mathrm{BW}_y$$

where γ is the gyromagnetic ratio, Δ*B* is the perturbation of the *B*0 field, and $\mathrm{FOV_y}$ and $\mathrm{BW_y}$ are the field of view and bandwidth, respectively. From this formula, we can conclude that the voxel shift in the phase-encoding direction will be inversely proportional to the effective bandwidth per voxel, which is consistent with our findings in the phantom: distortion was reduced using a higher bandwidth without altering any other acquisition parameter.

Parallel imaging reduces the number of phase-encoding steps, thus reducing the accumulating phase-encoding errors and resulting spatial distortions in SE-EPI. As shown in the brain (13,14), we demonstrated reduced geometric distortion when using parallel imaging (ie, higher acceleration factors).

In patients, the displacement ranged from 0 to 9.0 mm. This wide range may reflect the presence of variable *B*0 gradients in different patients. Reliable shimming before DWI acquisition probably plays a role in reducing *B*0 inhomogeneities. Unfortunately, filling the ERC balloon with barium sulfate did not seem to correct adequately for these inhomogeneities. The mean prostatic distortion was similar for the air and barium cohorts, although filling with air seemed to result in more variability as indicated by the larger range of distortion observed (ie, 0–9.0 mm with air vs. 0–4.2 mm with barium).

Another important observation in this study was that geometric distortion does not seem to depend on *b* values; this is critical because such distortion varied with different *b* values, the reliability of the ADC calculations could be jeopardized.

Alternative methods for reducing the EPI-related artifacts, including geometric distortion, have been proposed. One possible strategy is to apply segmented EPI pulse sequences (ie, multishot EPI); however, this approach increases acquisition time and is sensitive to patient motion. Jezzard et al. (11) described a postprocessing algorithm using a phase field map provided by a double-echo gradient recalled echo image in the brain. Others have used nonrigid registration methods to correct these distortions (12,13). Gholipour et al. (7) proposed a hybrid method consisting of field map–guided deformable registration of EPI to an undistorted T2-weighted sequence to correct the distortion. These strategies minimize distortion but depend on postprocessing steps. Errors from any of these steps (eg, field maps calculation) could degrade the final image.

Although some of our results might be anticipated based on theoretical background and previous investigations in other organs, to our knowledge, this is the first investigation assessing the degree of distortion in DWI of the prostate using a standard protocol with ERC at 3T. Furthermore, we assessed the parameters that may influence geometric distortion on SE-EPI DWI of the prostate. Some limitations, however, need to be discussed. First, some of the proposed remedies are already implemented in the clinical protocol for other purposes; regardless, our work substantiates efforts to further exploit accelerated imaging and increased bandwidth as tools to alleviate image deformation. The infusion of MRI scanners with a higher number of channels or digital systems accompanied by coils with dense array elements and unique geometries should allow for higher accelerations. Higher accelerations can allow for sequences with shorter echo trains to minimize the accumulation of phase errors. In addition, implementing DWI using a gradient and spin-echo sequence (14) may also reduce the accumulation of phase errors.

We also recognize that the strategies to correct the distortion were assessed in a phantom and therefore, the magnitude of these improvements in patients still needs to be determined. In patients, the range of distortion showed considerable variation, likely because of variable shimming. Moreover, the degree of distortion is expected to change depending on the image protocol used.

Of note, we did not appreciate an improvement in the geometric distortion by inflating the ERC with barium compared to patients in whom the ERC was inflated with air. This appears to be inconsistent with a previous report in which this strategy was used to improve the quality of spectroscopy data in the prostate by reducing the susceptibility gradients (9) and deservers further investigation. Agents such as barium sulfate and perfluorocarbon are used to inflate the ERC and reduce magnetic susceptibility gradients within the prostate secondary to the interface between air (traditionally used for coil inflation) and the surrounding tissues (15). Despite the lack of other studies validating such comparison, safety profile, lower cost, and availability of barium suspensions in clinical practice are appealing compared to perfluorocarbon (9). In the phantom, we chose to use the shimming process used in our clinical protocol to emulate the clinical scenario; however, the specific shimming method was not evaluated as part of this study. Further studies are necessary to fully understand the effect of different shimming algorithms on distortion and the relationship of these with the different strategies for inflating the ERC. Second, the geometric distortion on DWI is not the same throughout the image (11); we used the displacement between the prostate borders on DWI and T2-FSE images as a surrogate for the overall distortion. Although distortion was not measured using a pixel-by-pixel analysis, our method clearly demonstrated improvement by using accelerated imaging and higher bandwidths. Third, only partial correction of the distortion is achieved by the aforementioned strategies. For situations demanding better matches, such as radiology–genome or radiology–pathology correlation (16,17), other strategies that better mitigate the geometric distortion may be needed. Additional improvements may be necessary when considering the use of DWI for MRI-guided biopsies or focal therapy procedures (eg, high-intensity–focused ultrasound); displacements could lead to false-negative biopsy results, and incomplete ablation of tumor or inadvertent ablation of periprostatic tissue. Regardless, the

strategies proposed in this study may reduce targeting errors during prostate procedures and improve imaging coregistration.

In summary, geometric distortions are prevalent on single-shot SE-EPI DWI of the prostate. Strategies to reduce the distortion include the use of higher bandwidth and parallel imaging. Awareness of this artifact and potential remedies may result in improved mapping of prostate cancer. This reduction is particularly important in patients undergoing MRI-targeted biopsy and/or focal therapy.

ACKNOWLEDGMENTS

The authors would like to thank Dr. Evelyn Babcock, PhD, for her kind assistance with the phantom experiments.

REFERENCES

1. Kurhanewicz J, Vigneron D, Carroll P, et al. Multiparametric magnetic resonance imaging in prostate cancer: present and future. Curr Opin Urol. 2008; 18(1):71–77. [PubMed: 18090494]
2. Haider MA, van der Kwast TH, Tanguay J, et al. Combined T2-weighted and diffusion-weighted MRI for localization of prostate cancer. AJR Am J roentgenol. 2007; 189(2):323–328. [PubMed: 17646457]
3. Langer DL, van der Kwast TH, Evans AJ, et al. Prostate cancer detection with multi-parametric MRI: logistic regression analysis of quantitative T2, diffusion-weighted imaging, and dynamic contrast-enhanced MRI. JMRI. 2009; 30(2):327–334. [PubMed: 19629981]
4. Kozlowski P, Chang SD, Jones EC, et al. Combined diffusion-weighted and dynamic contrast-enhanced MRI for prostate cancer diagnosis—correlation with biopsy and histopathology. JMRI. 2006; 24(1):108–113. [PubMed: 16767709]
5. Woodfield CA, Tung GA, Grand DJ, et al. Diffusion-weighted MRI of peripheral zone prostate cancer: comparison of tumor apparent diffusion coefficient with Gleason score and percentage of tumor on core biopsy. AJR Am J of roentgenol. 2010; 194(4):W316–W322. [PubMed: 20308476]
6. Oto A, Yang C, Kayhan A, et al. Diffusion-weighted and dynamic contrast-enhanced MRI of prostate cancer: correlation of quantitative MR parameters with Gleason score and tumor angiogenesis. AJR Am J of roentgenol. 2011; 197(6):1382–1390. [PubMed: 22109293]
7. Gholipour A, Kehtarnavaz N, Scherrer B, et al. On the accuracy of unwarping techniques for the correction of susceptibility-induced geometric distortion in magnetic resonance Echo-planar images. Conf Proc IEEE Eng Med Biol Soc. 2011; 2011:6997–7000. [PubMed: 22255949]
8. Scherrer B, Gholipour A, Warfield SK. Super-resolution reconstruction to increase the spatial resolution of diffusion weighted images from orthogonal anisotropic acquisitions. Med Image Anal. 2012; 16(7):1465–1476. [PubMed: 22770597]
9. Rosen Y, Bloch BN, Lenkinski RE, et al. 3T MR of the prostate: reducing susceptibility gradients by inflating the endorectal coil with a barium sulfate suspension. Magn Reson Med. 2007; 57(5): 898–904. [PubMed: 17457870]
10. Hu Y, Ahmed HU, Taylor Z, et al. MR to ultrasound registration for image-guided prostate interventions. Med Image Anal. 2012; 16(3):687–703. [PubMed: 21216180]
11. Jezzard P, Balaban RS. Correction for geometric distortion in echo planar images from B0 field variations. Magn Reson Med. 1995; 34(1):65–73. [PubMed: 7674900]
12. Li Y, Xu N, Fitzpatrick JM, et al. Geometric distortion correction for echo planar images using nonrigid registration with spatially varying scale. Magn Reson Imaging. 2008; 26(10):1388–1397. [PubMed: 18499382]
13. Ardekani S, Sinha U. Geometric distortion correction of high-resolution 3 T diffusion tensor brain images. Magn Reson Med. 2005; 54(5):1163–1171. [PubMed: 16187289]
14. Oshio K, Feinberg DA. GRASE (gradient- and spin-echo) imaging: a novel fast MRI technique. Magn Reson Med. 1991; 20(2):344–349. [PubMed: 1775061]

15. Choi H, Ma J. Use of perfluorocarbon compound in the endorectal coil to improve MR spectroscopy of the prostate. AJR Am J of roentgenol. 2008; 190(4):1055–1059. [PubMed: 18356455]

16. Rutman AM, Kuo MD. Radiogenomics: creating a link between molecular diagnostics and diagnostic imaging. Eur J Radiol. 2009; 70(2):232–241. [PubMed: 19303233]

17. Zinn PO, Mahajan B, Sathyan P, et al. Radiogenomic mapping of edema/cellular invasion MRI-phenotypes in glioblastoma multiforme. PloS one. 2011; 6(10):e25451. [PubMed: 21998659]

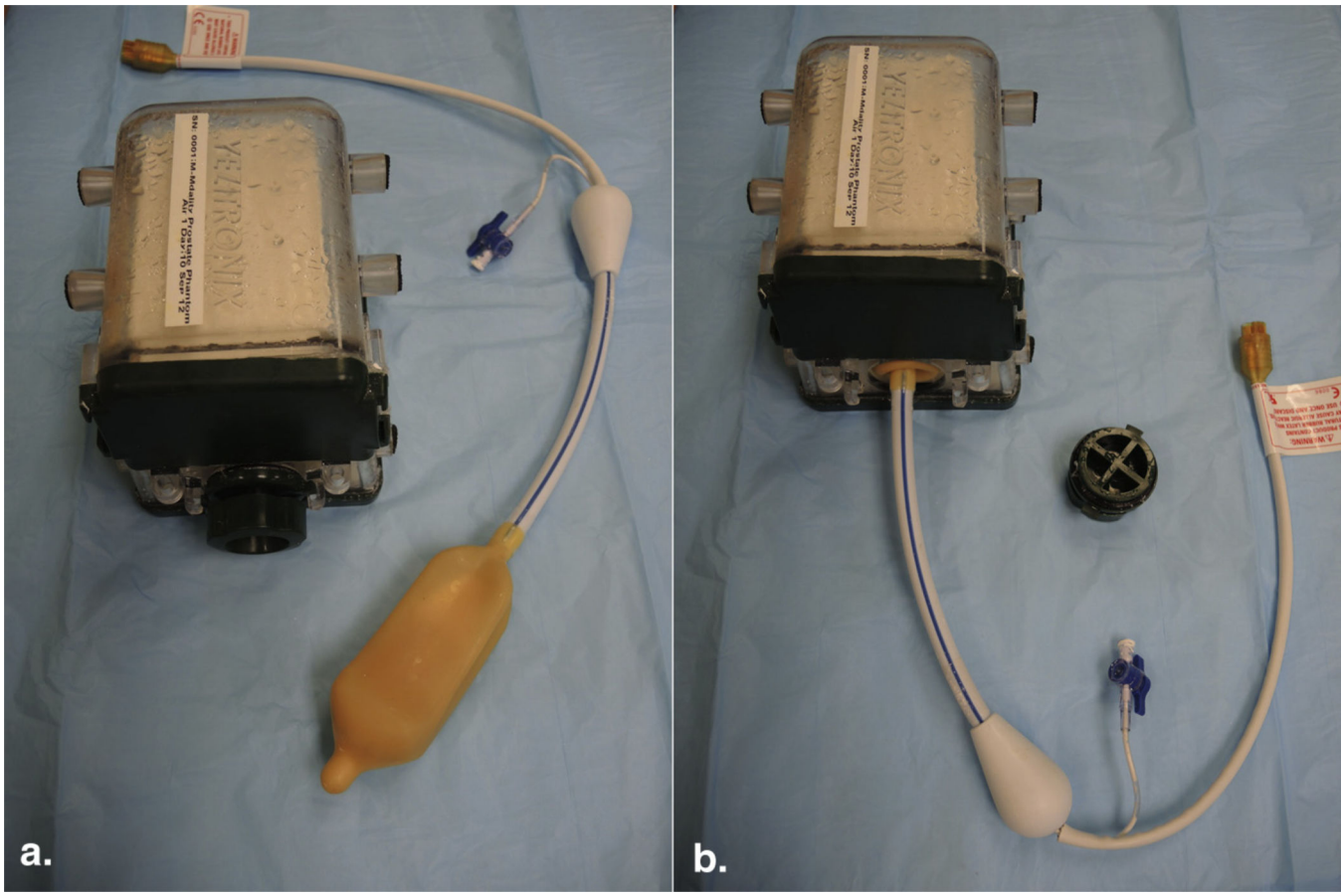

Figure 1.

(a) Prostate phantom model (Yezitronix Group Inc., Quebec, Canada) and endorectal coil (Medrad, Warrendale, PA). **(b)** The coil can be introduced in the phantom through a built-in orifice. (Color version of figure is available online.)

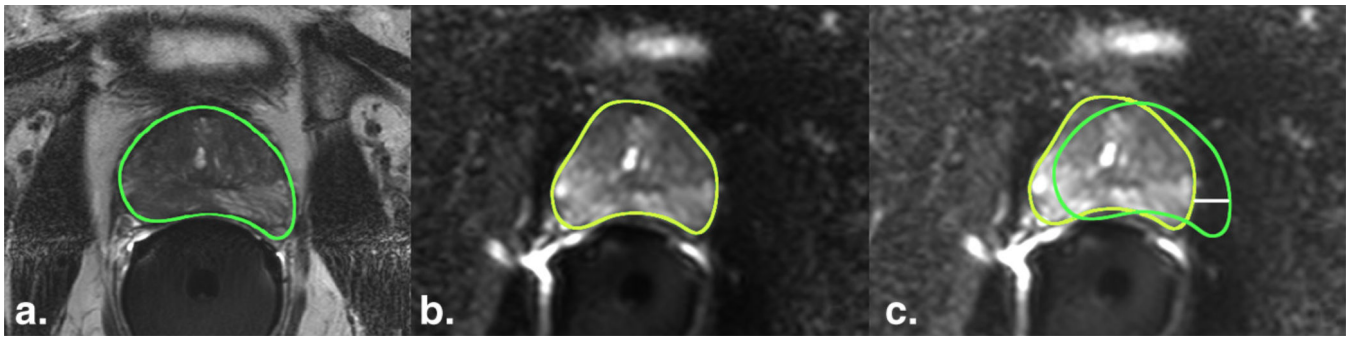

Figure 2.

Geometric distortion on diffusion-weighted imaging (DWI) in a patient. **(a)** The outer contour of the prostate in the T2-FSE image(TR, 8.2 seconds; TE, 120 milliseconds; flip angle, 90°) and **(b)** DWI image (TR, 6.8 seconds; TE, 76 milliseconds; flip angle, 90°) was delineated manually. The prostate contour from the T2-FSE image was saved and imported into the different *b*-value DWI images at the same anatomic level. **(c)** After overlapping the prostate contour from the T2-weighted reference image (*green*) on the DWI image (*yellow*), the geometric distortion was estimated by measuring the displacement between the boundaries in the horizontal axis (*white line*). FSE, fast spin-echo; TE, echo time; TR, repetition time. (Color version of figure is available online.)

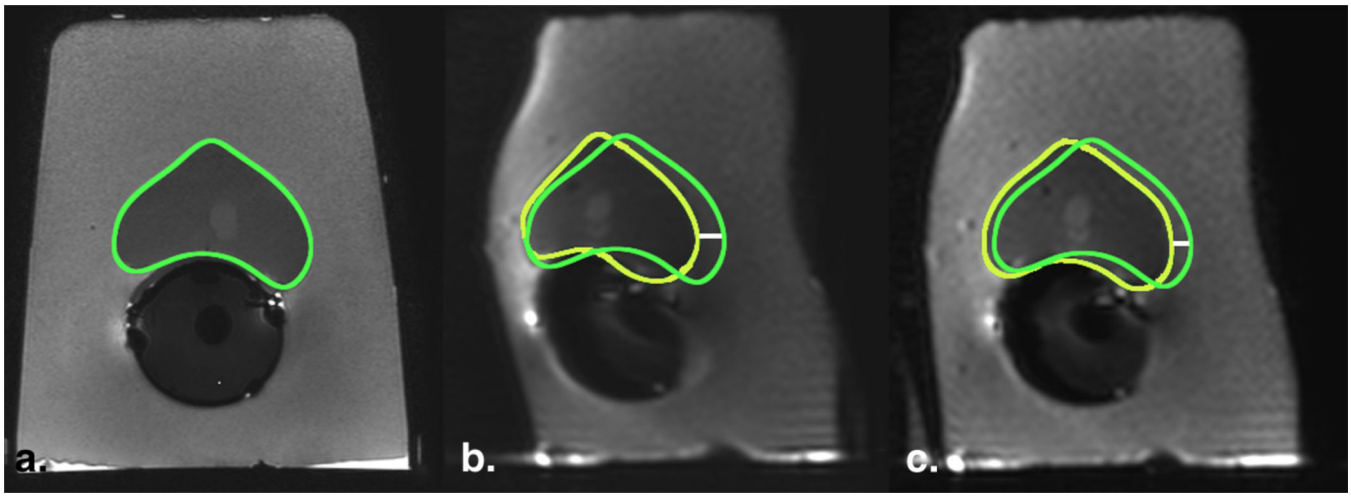

Figure 3.

Geometric distortion on diffusion-weighted imaging (DWI) in a phantom model decreases by increasing the acceleration factor. **(a)** T2-FSE image (TR, 8 seconds; TE, 120 milliseconds; flip angle, 90°) served as anatomic reference for the contour of the prostate (*green*);DWI images with **(b)** SENSE factor of 1 (TR, 10 seconds; TE, 93 milliseconds; flip angle 90°) and **(c)** SENSE factor of 2 (TR, 10 seconds; TE, 86 milliseconds; flip angle, 90°) were compared, showing a decrease in the displacement by increasing the acceleration factor. *Yellow* regions of interest indicate the outer contour of the prostate drawn on the DWI images; *white line* is the distance between the borders and represents magnitude of displacement (6 mm and 4m min **b** and **c**, respectively). FSE, fast spinecho; TE, echo time; TR, repetition time. (Color version of figure is available online.)

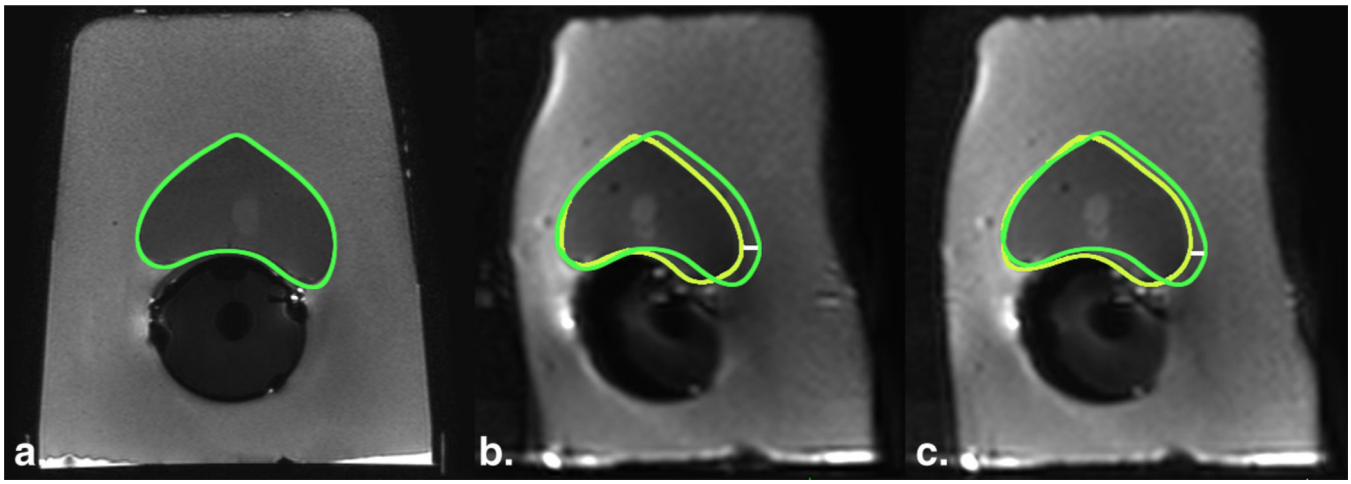

Figure 4.

Geometric distortion on diffusion-weighted imaging (DWI) in a phantom model decreases by increasing the bandwidth. **(a)** T2-FSE image (TR, 8 seconds; TE, 120 milliseconds; flip angle, 90°) served as anatomic reference for the contour of the prostate (*green*); DWI images with **(b)** bandwidth of 751 Hz/pixel (TR, 10 seconds; TE, 86 milliseconds; flip angle, 90°) and **(c)** 1252 Hz/pixel (TR, 10 seconds; TE, 75 milliseconds; flip angle, 90°) were compared, showing a decrease in the displacement of the contour by increasing the bandwidth. *Yellow* regions of interest indicate the outer contour of the prostate drawn on the DWI images; *white line* is the distance between the borders and represents magnitude of displacement (4.0 mm and 2.9 mm in **b** and **c**, respectively). FSE, fast spinecho; TE, echo time; TR, repetition time. (Color version of figure is available online.)

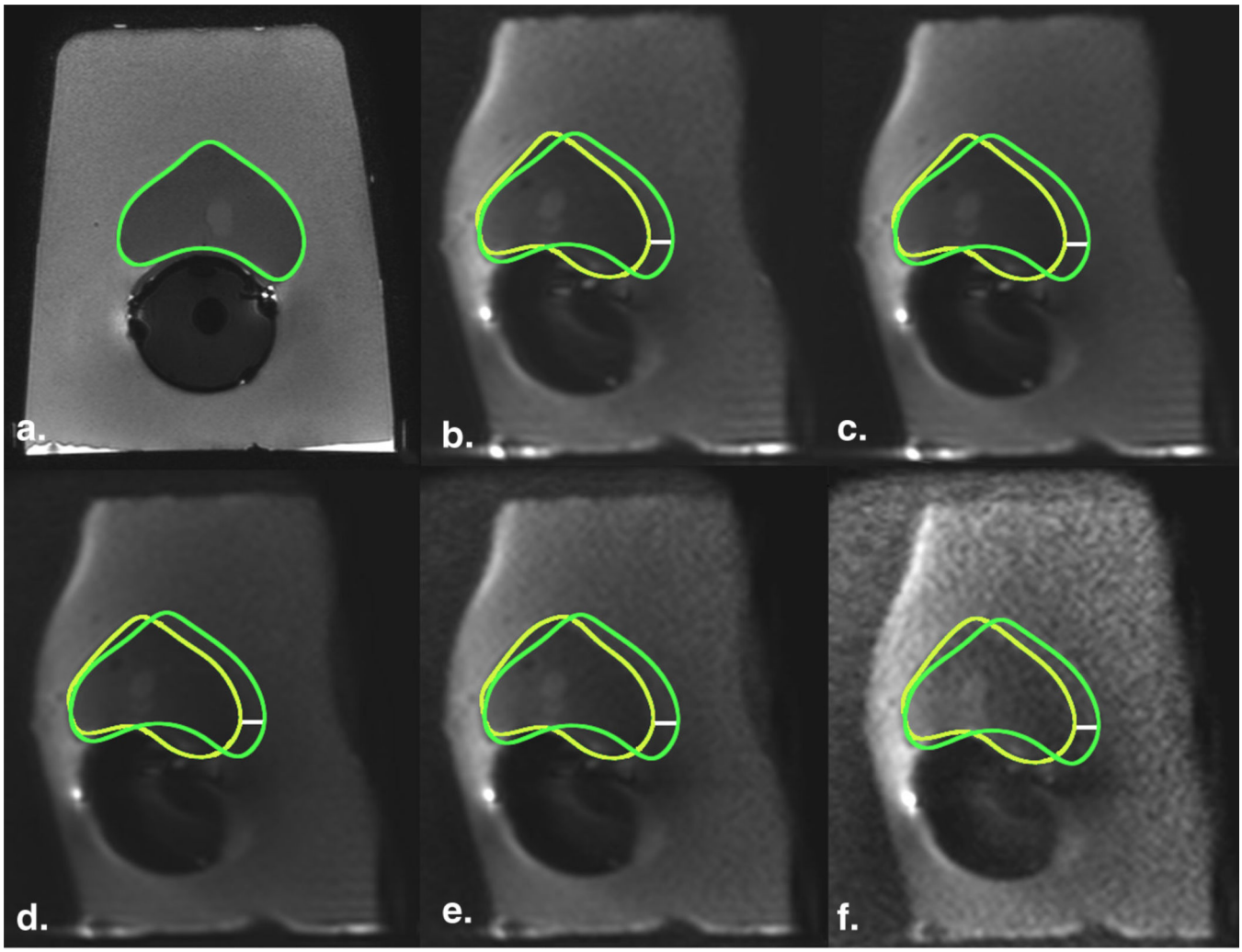

Figure 5.

Geometric distortion on diffusion-weighted imaging (DWI) in a phantom model does not change with the *b* value. **(a)** T2-FSE image (TR, 8 seconds; TE, 120 milliseconds; flip angle, 90) served as anatomic reference for the contour of the prostate (*green*); DWI images (TR, 10 seconds; TE, 99 milliseconds; flip angle, 90°) with *b* = 0 **(b)**, 40 **(c)**, 500 **(d)**, 1000 **(e)**, and 1500 **(f)** demonstrate the same degree of displacement. *Yellow* regions of interest indicate the outer contour of the prostate drawn on the DWI images; *white line* is the distance between the borders and represents magnitude of displacement (6.0 mm in all DWI images). FSE, fast spin-echo; TE, echo time; TR, repetition time. (Color version of figure is available online.)

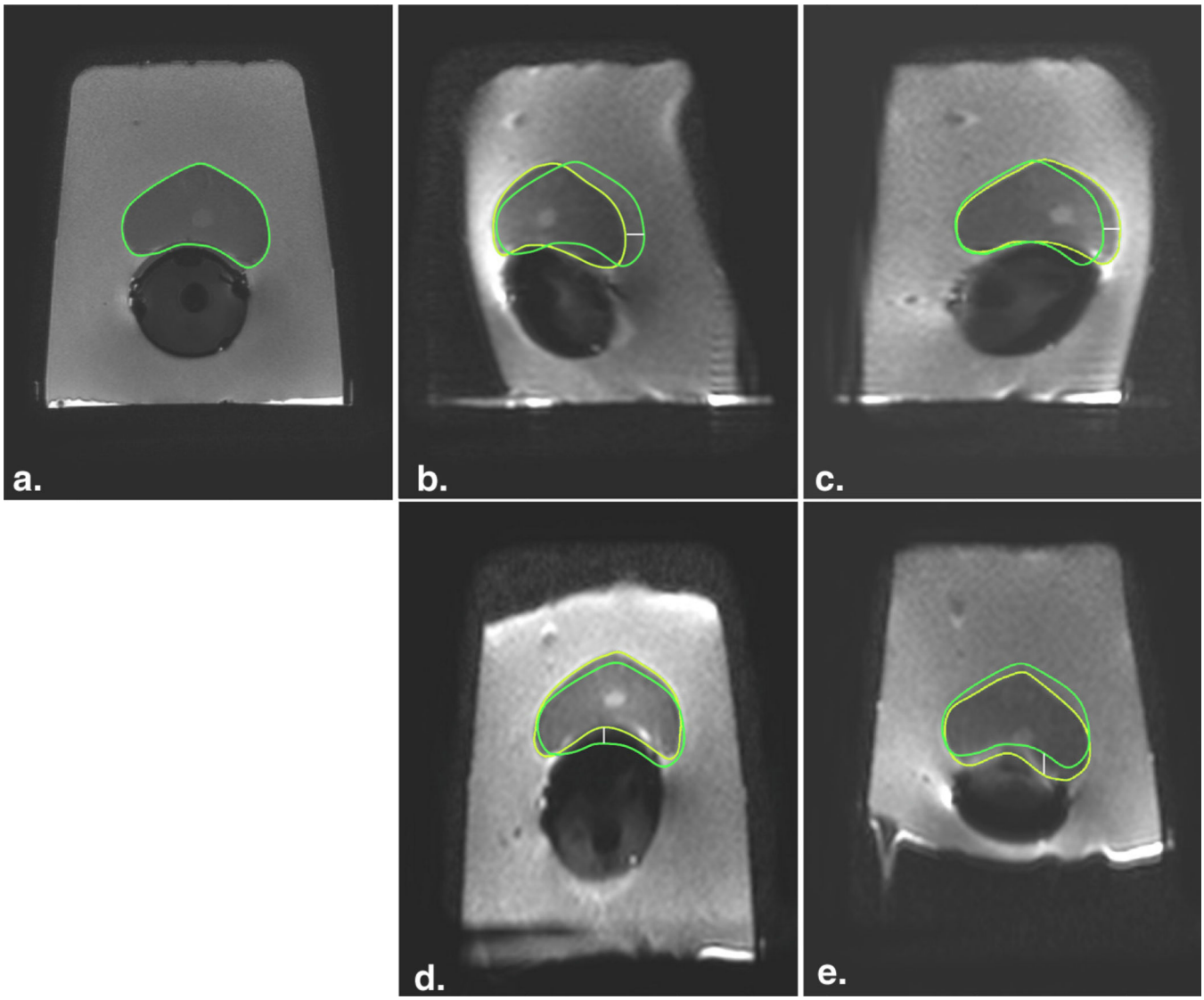

Figure 6.

Geometric distortion on diffusion-weighted imaging (DWI) in a phantom model occurs in the phase-encoding axis and direction. **(a)** T2-FSE image (TR, 8 seconds; TE, 120 milliseconds; flip angle, 90°) served as anatomic reference for the contour of the prostate (*green*); when the phase-encoding direction on DWI was shifted from right-to-left axis (TR, 10 seconds; TE, 99 milliseconds; flip angle, 90°; **b–c**) to the anterior-to-posterior axis (TR, 10 seconds; TE, 97 milliseconds; flip angle, 90°; **d–e**), the axis of the distortion consistently followed the phase-encoding direction. This effect can also be inferred by assessing the shape of the signal void in the endorectal balloon and the outer contour of the phantom. When the fat-shift direction was inverted, the distortion orientation was inverted (**b**, fat-shift left; **c**, fat-shift right; **d**, fat-shift posterior; and **e**, fat-shift anterior). *Yellow* regions of interest indicate the outer contour of the prostate drawn on the DWI images; *white line* is the

distance between the borders and represents magnitude of displacement. FSE, fast spin-echo; TE, echo time; TR, repetition time. (Color version of figure is available online.)

TABLE 1

Mean Displacement of the Prostate Boundaries between the T2-FSE and Diffusion-weighted Images Measured in the Left–Right Direction in Two Cohorts of Patients Undergoing Multiparametric MRI with the ERC Inflated with Air or Barium Sulfate

	***b* Value (s/mm^2)**	**Fat-shift**	**TE (milliseconds)**	**TR (milliseconds)**	**FOV (mm^2)**	**Reconstruction Matrix**	**Echo Train**	**SENSE Factor**	**BW (Hz/pixel)**	**Displacement (mm)**
Air (*n* = 20)	50	Left	75–78	6776–6955	180×180	144×140	73	2	1269–1392	1.8 (1.1)
	1000									1.7 (1.4)
Barium (*n* = 20)	50		76–77	6871–6954					1267–1339	1.7 (2.2)
	1000									1.8 (2.2)

BW, bandwidth; ERC, endorectal coil; FOV, field of view; FSE, fast spin-echo; TE, echo time; TR, repetition time.

Displacement values within parentheses reflect standard deviations.

TABLE 2

Displacement of the Prostate Boundaries between the T2-FSE and Diffusion-weighted Images in a Phantom Model with the ERC Filled with Barium

Test	Fat-shift	TE (milliseconds)	TR (milliseconds)	FOV (mm^2)	Matrix	Echo Train	SENSE Factor	BW (Hz/pixel)	Displacement (mm)
1	Left	99	10,000	180 × 180	144 × 141	141	1	1300	6.0
2	Right	99	10,000	180 × 180	144 × 141	141	1	1300	−4.6*
3	Posterior	97	10,000	180 × 180	144 × 141	141	1	1492	<1.0†
4	Anterior	97	10,000	180 × 180	144 × 141	141	1	1526	<1.0†
5	Left	93	10,000	160 × 160	128 × 124	125	1	1267	6.0
6	Left	86	10,000	160 × 160	128 × 124	65	2	751	4.0
7	Left	75	10,000	160 × 160	128 × 124	65	2	1253	2.9

BW, bandwidth; ERC, endorectal coil; FOV, field of view; FSE, fast spin-echo; TE, echo time; TR, repetition time.

In the tests 5–7, FOV was reduced to 160 × 160 mm^2 to allow broader variations in the BW.

*Negative value means reverse distortion orientation.

†Displacements were measured in the anterior–posterior axis with displacements <1 mm noted in the left–right axis. Standard deviation for the displacement not calculated given the limited number of phantom experiments under each condition.